



3-Dimensional non-fullerene acceptors based on triptycene and perylene diimide for organic solar cells



Yamin Zhang, Bin Kan, Xin Ke, Yunchuang Wang, Huanran Feng, Hongtao Zhang, Chenxi Li, Xiangjian Wan, Yongsheng Chen*

State Key Laboratory of Elemento-Organic Chemistry, Centre of Nanoscale Science and Technology and Key Laboratory of Functional Polymer Materials, College of Chemistry, Nankai University, Tianjin, 300071, China

ARTICLE INFO

Article history:

Received 21 April 2017
Received in revised form
11 July 2017
Accepted 11 July 2017
Available online 15 July 2017

Keywords:

Organic solar cell
Non-fullerene acceptor
Three-dimensional
Triptycene
Perylene diimide

ABSTRACT

Two molecules based on triptycene and perylene diimide (PDI) were designed and synthesized as non-fullerene acceptors for organic solar cells (OSCs). The bay-substituted and the imide-substituted molecules, named as TPBA and TPI, respectively, have rigid three-dimensional backbones, which improved the morphological compatibility with the donor polymers. TPBA and TPI exhibit suitable energy levels as acceptors and efficient absorption in the range of 450–600 nm. Their blended films with PTB7-Th displayed power conversion efficiencies of 2.80% and 3.64%, respectively.

© 2017 Elsevier B.V. All rights reserved.

1. Introduction

Organic solar cells (OSCs) with bulk hetero junction (BHJ) architecture are under intense study because they have the bright future in producing low-cost large area solar cells via solution methods on flexible substrates [1–4]. Presently, power conversion efficiencies (PCEs) over 10% have been achieved for single junction OSCs with fullerene derivatives as acceptors [5–10]. Fullerene derivatives have plenty of advantages such as high electron affinity, high electron mobility, isotropic charge transport and favourable nanoscale network forming behaviours [11,12]. However, their drawbacks could not be negligible, such as the restricted electronic tuning ability, weak absorption in the visible region and high cost of production and purification.

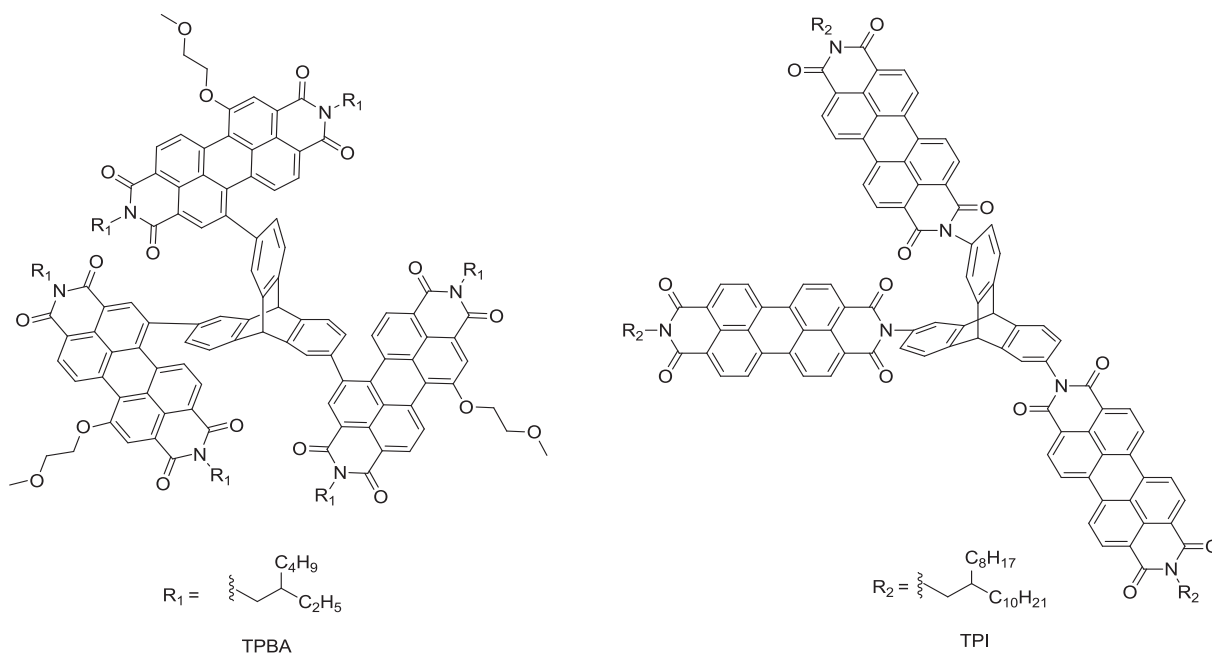
Recently, non-fullerene BHJ solar cells with PCEs >11% have been reported, indicating the potential of non-fullerene acceptors (NFAs) [13–18]. Among the family of NFAs, perylene diimide (PDI) derivatives, which possess high thermal/photochemical stabilities, efficient absorption intensity in the visible region (400–600 nm), are one of the ideal candidates for the substitution of fullerene

derivatives [19–24]. However, the individual PDI molecules have strong intermolecular interactions induced by a highly planar conformation, which will lead to strong self-assembling and thus the undesired large crystalline domains. Recently, great efforts have been paid to break the self-assembling of PDI groups [25–29]. Among these methods, constructing a three dimensional (3D) structure is an effective way to decrease the crystallinity of the PDI-based acceptors and to form an extended π -conjugated framework, and thus isotropic charge transport [30–35].

Herein, we report two three dimensional PDI acceptors using triptycene as the core building block due to its unique rigid, contorted, fully aromatic structure. In triptycene, three aromatic benzene units formed a 3D rigid paddle wheel shape, thus it could be an ideal scaffold to place three electron acceptor units. Furthermore, photoelectron spectroscopy studies suggest that there is an electronic communication between the three benzene units of triptycene by homoconjugation [36–39]. This might be helpful for better charge separation and transportation. The bay-substituted molecule and the imide-substituted molecule were named as TPBA and TPI, respectively (Scheme 1). The influences of molecular geometry on the OSC performance were investigated by studying their optical, photophysical and morphological properties in the BHJ blended films with PTB7-Th.

* Corresponding author.

E-mail address: yschen99@nankai.edu.cn (Y. Chen).



Scheme 1. The chemical structures of TPBA and TPI.

2. Experimental section

2.1. Materials and synthesis

All reactions and manipulations were carried out under argon atmosphere with the use of standard Schlenk techniques. All starting materials were purchased from commercial suppliers and used without further purification unless indicated otherwise. Compound 1, 2, 3 and 4 were synthesized according to the literature [40–43].

2.1.1. TPBA

A solution of compounds 1 (150 mg, 0.24 mmol) and 2 (737 mg, 0.96 mmol) in toluene (45 mL) and aqueous 2 M Na_2CO_3 (15 mL) was degassed twice with argon. Then $\text{Pd}(\text{PPh}_3)_4$ (50 mg, 0.043 mmol) was added and the mixture was stirred at 100 °C for 24 h under argon, after which the mixture was poured into water (200 mL), and extracted with chloroform. The organic layer was washed with water, and then dried over anhydrous Na_2SO_4 . The solvent was removed by rotating evaporator and the residue was purified by silica gel chromatography using a mixture of CHCl_3 :acetone (8:1) eluent to produce compound TPBA (204 mg, 36.8%). ^1H NMR (400 MHz, CDCl_3): δ 8.27–8.61 (m, 9H), 7.40–8.11 (m, 18H), 5.54–5.70 (d, 2H), 4.42–4.59 (m, 6H), 4.14–4.15 (m, 6H), 3.93–3.98 (m, 9H), 3.41–3.59 (m, 12H), 1.78–1.99 (m, 6H), 1.25–1.35 (m, 48H), 0.84–0.98 (m, 36H). MS (MALDI-TOF): calcd for $\text{C}_{149}\text{H}_{152}\text{N}_6\text{O}_{18}$ [M^+], 2314.83; found: 2314.11. Anal. calcd. for $\text{C}_{149}\text{H}_{152}\text{N}_6\text{O}_{18}$: C 77.24%, H 6.56%, N 3.62%, found: C 76.66%, H 6.85%, N 3.43%.

2.1.2. TPI

Compound 3 (45 mg, 0.15 mmol), compound 4 (400 mg, 0.59 mmol) and $\text{Zn}(\text{OAc})_2 \cdot 2\text{H}_2\text{O}$ (0.12 mg) were suspended in quinoline (2 mL) and heated up at 180 °C for 24 h under argon. The resulting brownish solution was washed with aq HCl (18%) (80 mL) and the aqueous phase was extracted with DCM (2 × 20 mL). The combined organic phase was dried over Na_2SO_4 , concentrated under reduced pressure and separated by column chromatography with CHCl_3 :acetone (100:1) as eluent, TPI was obtained as red solid

(yield: 57.8%, 195 mg, 0.086 mmol). MS (MALDI-TOF): calcd for $\text{C}_{152}\text{H}_{158}\text{N}_6\text{O}_{12}$ [M^+], 2260.91; found: 2260.17. Anal. calcd. for $\text{C}_{152}\text{H}_{158}\text{N}_6\text{O}_{12}$: C 80.67%, H 6.98%, N 3.71%, found: C 80.75%, H 7.12%, N 3.52%.

2.2. Instruments and characterization

The ^1H and ^{13}C NMR spectra were recorded on a Bruker AV400 Spectrometer. Matrix assisted laser desorption/ionization time-of-flight mass spectrometry (MALDI-TOF) were performed on a Bruker Autoflex III LRF200-CID instrument. The thermo gravimetric analysis (TGA) and differential scanning calorimetry (DSC) were carried out on a NETZSCH STA 409PC instrument under purified nitrogen gas flow. The heating rate for TGA and DSC testing is 10 °C min^{-1} , and the cooling rate for DSC is 10 °C min^{-1} . UV–Vis spectra were obtained with a JASCO V-570 spectrophotometer.

Cyclic voltammetry (CV) experiments were performed with a LK2010 electrochemical workstation. All CV measurements were carried out at room temperature with a conventional three-electrode configuration employing a glassy carbon electrode as the working electrode, a saturated calomel electrode (SCE) as the reference electrode, and a Pt wire as the counter electrode. Dichloromethane was distilled from calcium hydride under dry nitrogen immediately prior to use. Tetrabutylammonium phosphorus hexafluoride (Bu_4NPF_6 , 0.1 M) in dry dichloromethane was used as the supporting electrolyte, and the scan rate was 100 mV s^{-1} . The lowest unoccupied molecular orbital (LUMO) energy levels were calculated from the onset reduction potential, using the equation $E_{\text{LUMO}} = -(E_{\text{red, onset}} + 4.8)$ eV. The HOMO energy levels were calculated from LUMO and $E_{\text{g}}^{\text{opt}}$ by formula $E_{\text{HOMO}} = (E_{\text{LUMO}} - E_{\text{g}}^{\text{opt}})$ eV.

The geometry structures of TPBA and TPI were optimized by using DFT calculations (B3LYP/6-31G*), and the frequency analysis was followed to assure that the optimized structures were stable states. All calculations were carried out using Gaussian 09.

Atomic force microscopy (AFM) was performed using Multi-mode 8 atomic force microscope in tapping mode. The transmission electron microscopy (TEM) investigation was performed on Philips

Technical G² F20 at 200 kV. The specimen for TEM measurement was prepared by spin casting the blend solution on ITO/PEDOT:PSS substrate, then floating the film on a water surface, and transferring to TEM grids. Photoluminescence characterization is carried out using a FluoroMax-P luminescence spectrometer using a xenon lamp as the source of excitation. The excitation wavelength is 460 nm.

Space charge limited current (SCLC) mobility was measured using a diode configuration of ITO/PEDOT:PSS/PTB7-Th:TPBA (TPI)/Au for hole mobility and glass/Al/PTB7-Th:TPBA (TPI)/Al for electron mobility and fitting the results to a space charge limited form, where SCLC equation is described by:

$$J = \frac{9\epsilon_0\epsilon_r\mu_0V^2}{8L^3} \exp\left(0.89\beta\sqrt{\frac{V}{L}}\right)$$

where J is the current density, L is the film thickness of the active layer, μ_0 is the mobility, ϵ_r is the relative dielectric constant of the transport medium, ϵ_0 is the permittivity of free space (8.85×10^{-12} F m⁻¹), $V (= V_{\text{app}} - V_{\text{bi}})$ is the internal voltage in the device, where V_{app} is the applied voltage to the device and V_{bi} is the built-in voltage due to the relative work function difference of the two electrodes.

2.3. Solar cell fabrication and testing

The devices were fabricated with a structure of glass/ITO/PEDOT:PSS/PTB7-Th: acceptors/ETL/Al. The ITO-coated glass substrates were cleaned by ultrasonic treatment in detergent, deionized water, acetone, and isopropyl alcohol under ultra-sonication for 15 min each and subsequently dried by a nitrogen blow. A thin layer of PEDOT: PSS (Clevios P VP Al 4083, filtered at 0.45 μm) was spin-coated at 4000 rpm onto ITO surface. After baked at 150 °C for 20 min, the substrates were transferred into an argon-filled glove box. Subsequently, the active layer was spin-coated from blend chloroform solutions of PTB7-Th: TPBA (2% 1-Naphthalenethiol, 140 °C annealing 10 min) and PTB7-Th: TPI (3% 1, 8-Diiodooctane), respectively. Finally, a thin layer of electron transport layer including ZnO nanoparticles, PrC₆₀-MA and PDIN were spin-coated and 80 nm Al layer were deposited under high vacuum ($<2 \times 10^{-4}$ Pa). The effective areas of cells were 4 mm² defined by shadow masks. The current density-voltage (J - V) curves of photovoltaic devices were obtained by a Keithley 2400 source-measure unit. The photocurrent was measured under illumination simulated 100 mW cm⁻² AM 1.5G irradiation using a SAN-EI XES-70S1 solar simulator, calibrated with a standard Si solar cell. External quantum efficiencies were measured using a lock-in amplifier (SR810, Stanford Research Systems). The devices were illuminated by monochromatic light from a 150 W xenon lamp passing through an optical chopper and a monochromator. Photon flux was determined by a calibrated standard silicon photodiode.

3. Results and discussion

3.1. Materials synthesis and characterization

The synthetic routes of TPBA and TPI are illustrated in Scheme 2, and the detailed synthetic procedures and characterization data are presented in the experimental section. Compound 1, 2, 3 and 4 were synthesized according to the literature, respectively [40–43]. The chemical structure and purity of TPBA was confirmed by NMR, elemental analysis, and Time-off light (MALDI-TOF) MS. TPI didn't show satisfying NMR spectra due to its expanded π -structure [44], but its chemical structure and purity could be confirmed by elemental analysis, MALDI-TOF MS and HPLC (see Figs. S7–S8 in

supporting information). These two molecules both exhibit good solubility in chloroform.

Theoretical calculations were then performed using density functional theory (DFT) at the B3LYP/6-31G(d) level to understand the electron distribution in TPBA and TPI. As shown in Fig. S1, TPBA and TPI both show non-planar 3-D structure mainly due to the unique structure of triptycene, which could effectively avoid the over self-aggregation of PDI unit. For TPBA molecule, low-density π -electrons were extended to the benzene of the triptycene core, and each PDI unit is not coplanar with the corresponding phenyl groups in triptycene unit. The torsion angles are about 55.8°, 54.5°, 53.7°, respectively. For TPI molecule, the torsion angles are about 85.0°, 89.8°, 94.6°, but the π -electrons are only distributed on the three PDI units because the imide-linkage blocks the extension of electrons [45].

Thermo gravimetric analysis (TGA) results suggest that both two molecules exhibit good thermal stability, which is necessary for the application in OPVs (see Fig. 1). Their solid state thermal transitions were determined by differential scanning calorimetry (DSC) analysis as shown in Fig. 1c and d. From their DSC plots, it can be seen that no obvious melting temperatures (T_m) and recrystallization (T_{cr}) points are obtained for both molecules, indicating that they are not easy to crystallize.

3.2. Optical absorption and electrochemical properties

Cyclic voltammetry (CV) was performed to investigate the electrochemical properties of TPBA and TPI (Fig. 2a and b and Table 1). The LUMO energy levels of TPBA and TPI were estimated to be -3.72 and -3.76 eV from the reduction potential by using the empirical formula, $E_{\text{LUMO}} = -(E_{\text{red, onset}} + 4.8)$ eV, assuming the absolute energy level of FeCp₂^{+/0} to be 4.8 eV below vacuum. The optical band gaps (E_g^{opt}) of TPBA and TPI are 1.96 and 2.13 eV, respectively, which were estimated from their film absorbance cut off wavelength. The HOMO energy levels of TPBA and TPI are calculated to be -5.68 and -5.89 eV from their LUMO and E_g^{opt} by formula $E_{\text{HOMO}} = (E_{\text{LUMO}} - E_g^{\text{opt}})$ eV. These results suggest that both molecules possess suitable energy levels as electron acceptors.

The UV–Vis absorption spectra of TPBA and TPI are depicted in Fig. 2c and d and their corresponding data are summarized in Table 1. The maximum molar extinction coefficient (ϵ) of TPBA and TPI are 4.8×10^4 M⁻¹cm⁻¹ at 571 nm and 4.42×10^4 M⁻¹cm⁻¹ at 530 nm in their solution state, respectively. The absorption spectra of both TPBA and TPI in the film states were broadened compared to the solution states. When blended with PTB7-Th donor, effective complementary absorption covered range from 400 to 800 could be obtained.

3.3. Photovoltaic performance

BHJ organic solar cells were fabricated using PTB7-Th as the electron donor material and the two new molecules as the electron acceptors material with a device structure of ITO/PEDOT: PSS/PTB7-Th: acceptors/ZnO/Al (Fig. 3). The optimization process of the device performance can be found in Tables S1–S8. The optimized processing condition for PTB7-Th: TPBA based devices is D/A weight ratio of 1: 0.8 with 2% HS-N (1-Naphthalenethiol) as additive and thermal annealing at 140 °C for 10 min. For PTB7-Th: TPI based devices, the optimal processing condition is D/A weight ratio of 1: 1 with 3% DIO (1, 8-diiodooctane) as additive. The optimized photovoltaic parameters of the two molecules based devices were summarized in Table 2.

As shown in Fig. 4a, the TPBA based OSCs exhibited a maximum power conversion efficiency (PCE) of 2.80% with a short circuit current density (J_{sc}) of 8.03 mA/cm², an open-circuit voltage (V_{oc}) of

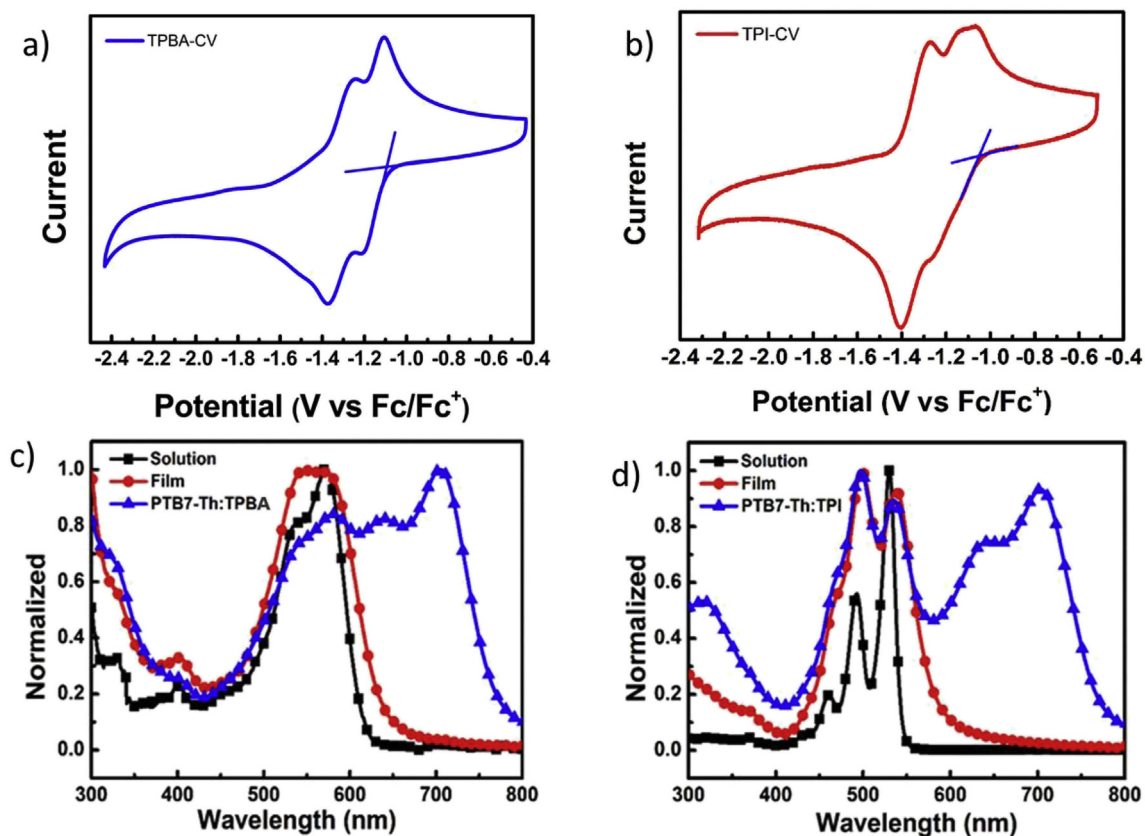


Fig. 2. a, b) Cyclic voltammograms of TPBA and TPI in dichloromethane solutions; c, d) UV-vis absorption spectra of TPBA and TPI in chloroform solutions, thin films and blended films with PTB7-Th.

Table 1
Optical and electrochemical data of compounds TPBA and TPI.

molecules	$\lambda_{\max, \text{sol}}$ [nm]	ϵ_{sol} [$\text{M}^{-1} \text{cm}^{-1}$]	$\lambda_{\max, \text{film}}$ [nm]	$E_{\text{g}}^{\text{opt, film}}$ [eV]	HOMO [eV] ^a	LUMO [eV]
TPBA	571	4.8×10^4	547	1.96	-5.68 ^a	-3.72
TPI	530	4.4×10^4	498, 537	2.13	-5.89 ^a	-3.76

^a Calculate from E_{LUMO} and $E_{\text{g}}^{\text{opt}}$, $E_{\text{g}}^{\text{opt}}$ is calculated from film absorbance cut off wavelength.

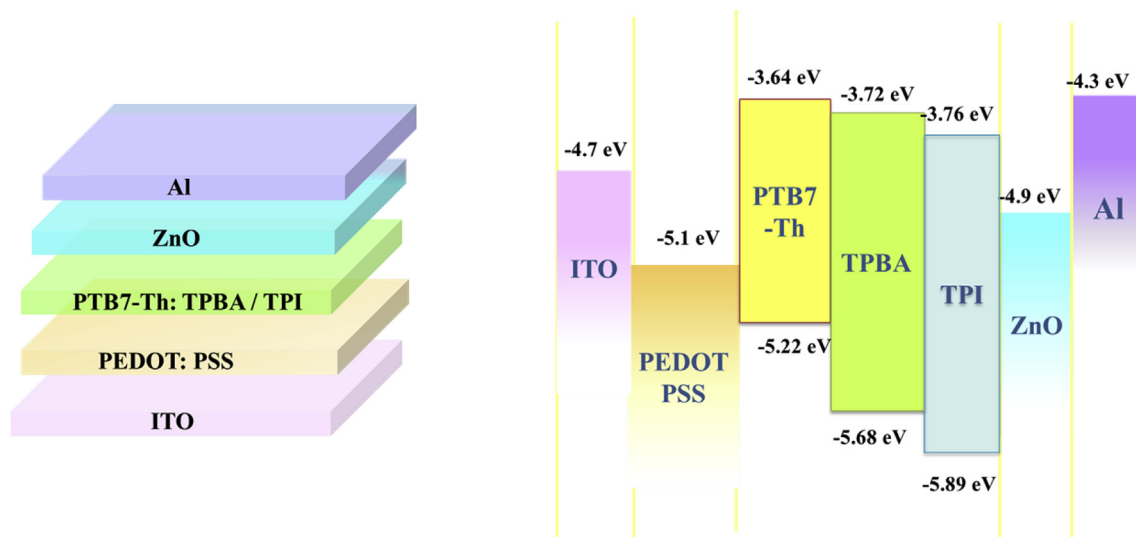


Fig. 3. The device architecture and energy diagram of the solar cell.

Table 2
The optimized photovoltaic performance of TPBA and TPI based devices.

molecules	V_{oc} [V]	J_{sc} [mA cm^{-2}]	FF	PCE [%]
TPBA ^a	0.889	8.03	0.387	2.80
TPI ^b	0.777	9.63	0.486	3.64

^a 2% HS-N, 140 °C thermal annealing.

^b 3% DIO.

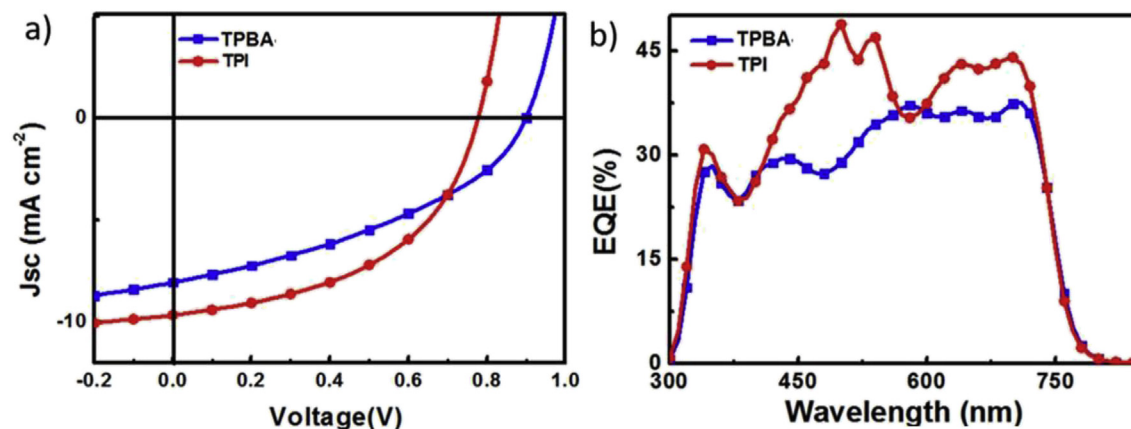


Fig. 4. a) Characteristic current density versus voltage (J - V) curves of the optimized devices based on TPBA and TPI under simulated AM 1.5 G irradiation (100 mW cm^{-2}). b) The external quantum efficiency (EQE) curves of the optimized devices.

PTB7-Th and TPI, which leads to a higher V_{oc} of TPBA. The offset between LUMO level of PTB7-Th and LUMO level of TPBA is narrower than that between PTB7-Th and TPI. The stronger electron transport driving force contributed to the increased J_{sc} and FF values. Fig. 4b shows the external quantum efficiency (EQE) spectra of the optimum devices. The EQE responses covered a wavelength

and PTB7-Th:TPI show root-mean-square (rms) surface roughness of 2.55 and 2.28 nm, respectively, and the rms roughness of their optimized films decrease to 0.68 and 0.62 nm, which reveals that the optimized films are smooth with high quality. TEM studies (Fig. 6) showed that without any treatment, both PTB7-Th:TPBA and PTB7-Th:TPI blend films show no obvious phase separation of

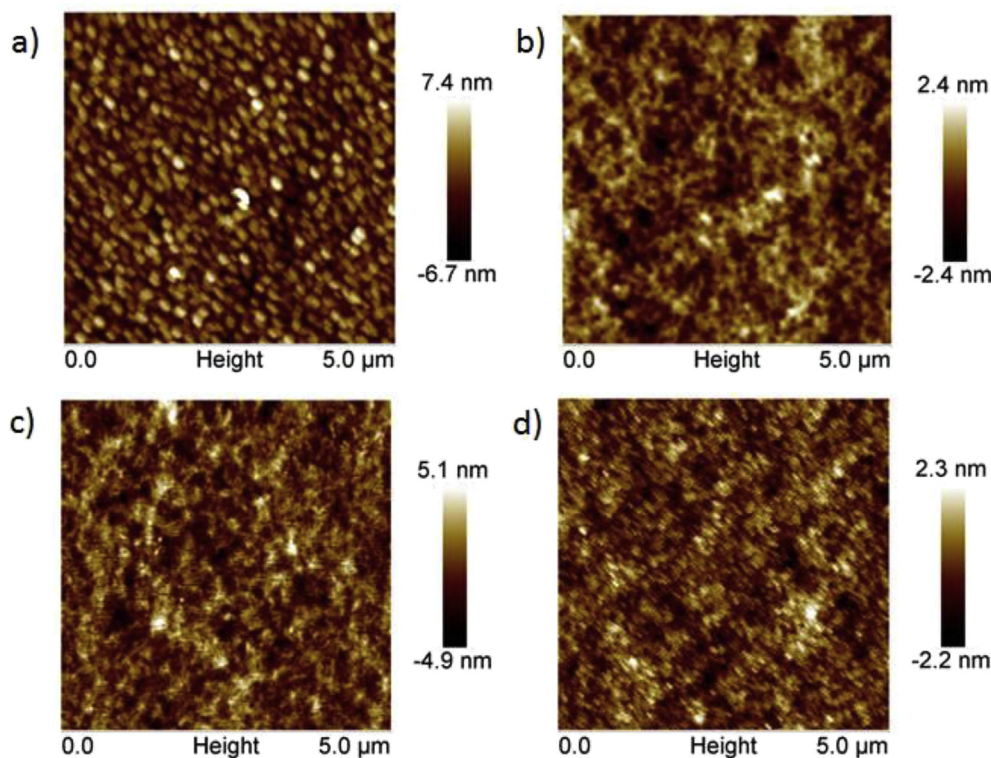


Fig. 5. Tapping-mode AFM height images of (a, b) PTB7-Th: TPBA (1: 0.8, w/w); (c, d) PTB7-Th: TPI (1: 1, w/w). (Panels a, c show the blend films without post-treatment; panels b show the PTB7-Th: TPBA blend films with 2% HS-N as additive and thermal annealing at 140 °C for 10 min; panels d show the PTB7-Th: TPI blend films with 3% DIO as additive).

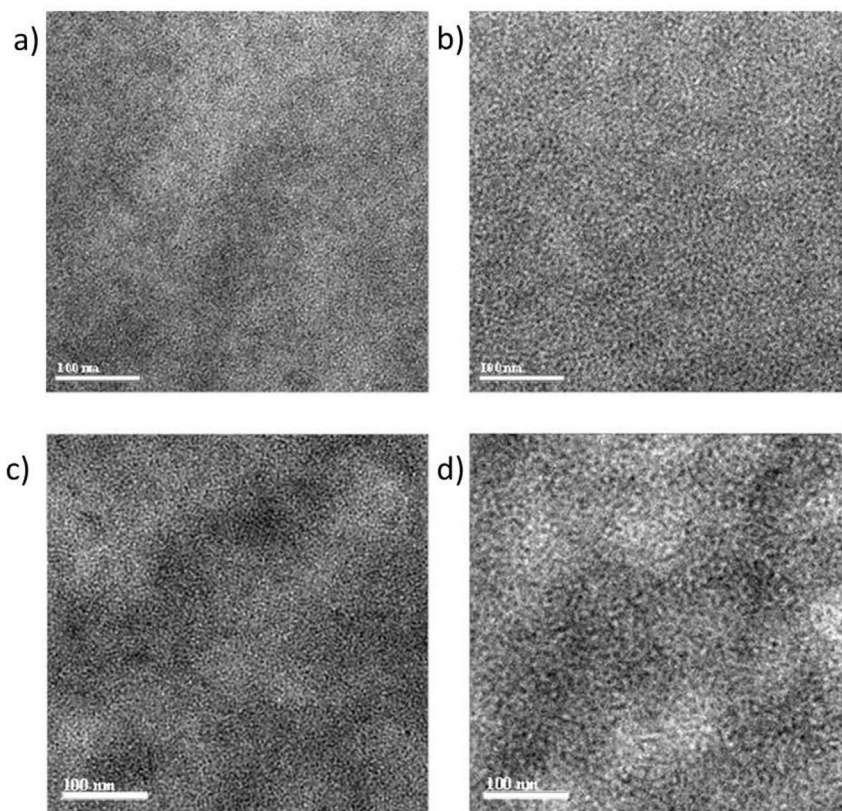


Fig. 6. TEM images of (a, b) PTB7-Th: TPBA (1: 0.8, w/w); (c, d) PTB7-Th: TPI (1: 1, w/w). (Panels a, c show the blend films without post-treatment; panels b show the PTB7-Th: TPBA blend films with 2% HS-N as additive and thermal annealing at 140 °C for 10 min; panels d show the PTB7-Th: TPI blend films with 3% DIO as additive).

the donor and acceptor, which could be unfavorable for charge transport, thus leading to low J_{sc} and FF. After post treatments, the PTB7-Th:TPBA blend films showed a larger domain size of 5–10 nm than their pristine films, and PTB7-Th:TPI blend films exhibited homogeneous interpenetrating networks with a domain size of 10–20 nm, the domain size of PTB7-Th:TPI blend films is closer to the exciton diffusion length, and leading to a better device performance than PTB7-Th:TPBA based devices.

The molecular packing states of pure TPBA and TPI films were studied by X-ray diffraction (XRD) analysis (Fig. S2). There are no clear peaks in the XRD patterns of these two molecules, indicating their amorphous nature, which illustrate constructing three dimensional (3D) structure is an effective way to decrease the crystallinity of the PDI-based acceptors.

The mobilities of the optimized devices were measured by the space charge limited current (SCLC) method (Fig. S3). The hole and electron mobilities for TPBA-based devices are 4.03×10^{-5} and $6.53 \times 10^{-5} \text{ cm}^2 \text{ V}^{-1} \text{ s}^{-1}$, respectively. For TPI based devices, the hole and electron mobilities are 5.43×10^{-5} and $7.98 \times 10^{-5} \text{ cm}^2 \text{ V}^{-1} \text{ s}^{-1}$, respectively. The low charge carrier mobilities are detrimental for charge transport and collection, thus lead to their low J_{sc} and FF values, which are contributed to the overall low device performances.

4. Conclusion

In conclusion, we have synthesized two 3D acceptor molecules based on triptycene and perylene diimide (PDI). When blended with PTB7-Th, TPBA based devices exhibited a maximum power conversion efficiency of 2.80% with a J_{sc} of 8.03 mA/cm^2 , V_{oc} of 0.889 V and FF of 0.387. And the TPI based devices demonstrated a

maximum power conversion efficiency of 3.64% with a J_{sc} of 9.63 mA/cm^2 , V_{oc} of 0.777 V and FF of 0.486. They all have 3D interlocking geometry, which improve the morphological compatibility with the donor polymers, yielded smooth and homogeneous blend thin films that favoured the interpenetrating BHJ morphology. These results demonstrate that constructing 3D electron-accepting materials is one of effective ways to achieve efficient photovoltaic performances.

Acknowledgments

The authors gratefully acknowledge the financial support from MOST (2014CB643502) and NSF (91433101, 51422304, 51373078) of China and Tianjin city (17JCZDJC31100).

Appendix A. Supplementary data

Supplementary data related to this article can be found at <http://dx.doi.org/10.1016/j.orgel.2017.07.021>.

References

- [1] G. Yu, J. Gao, J. Hummelen, F. Wudl, A. Heeger, *Nature* 425 (2003) 158.
- [2] A.C. Arias, J.D. MacKenzie, I. McCulloch, J. Rivnay, A. Salleo, *Chem. Rev.* 110 (2010) 3.
- [3] G. Dennler, M.C. Scharber, C.J. Brabec, *Adv. Mater* 21 (2009) 1323.
- [4] S.B. Darling, F. You, *Rsc Adv.* 3 (2013) 17633.
- [5] J.D. Chen, C. Cui, Y.Q. Li, L. Zhou, Q.D. Ou, C. Li, Y. Li, J.X. Tang, *Adv. Mater* 27 (2015) 1035.
- [6] Z. He, B. Xiao, F. Liu, H. Wu, Y. Yang, S. Xiao, C. Wang, T.P. Russell, Y. Cao, *Nat. Phot.* 9 (2015) 174.
- [7] B. Kan, M. Li, Q. Zhang, F. Liu, X. Wan, Y. Wang, W. Ni, G. Long, X. Yang, H. Feng, *J. Am. Chem. Soc.* 137 (2015) 3886.
- [8] S. Zhang, L. Ye, W. Zhao, B. Yang, Q. Wang, J. Hou, *Sci. China Chem.* 58 (2015)

- 248.
- [9] Y. Liu, J. Zhao, Z. Li, C. Mu, W. Ma, H. Hu, K. Jiang, H. Lin, H. Ade, H. Yan, *Nat. Commun.* 5 (2014).
- [10] C. Liu, C. Yi, K. Wang, Y. Yang, R.S. Bhatta, M. Tsige, S. Xiao, X. Gong, *ACS Appl. Mater. Interfaces* 7 (2015) 4928.
- [11] Y. He, Y. Li, *Phys. Chem. Chem. Phys.* 13 (2011) 1970.
- [12] D.M. Guldi, B.M. Illescas, C.M. Atienza, M. Wielopolski, N. Martín, *Chem. Soc. Rev.* 38 (2009) 1587.
- [13] H. Bin, L. Gao, Z.-G. Zhang, Y. Yang, Y. Zhang, C. Zhang, S. Chen, L. Xue, C. Yang, M. Xiao, Y. Li, *Nat. Commun.* 7 (2016) 13651.
- [14] S. Dai, F. Zhao, Q. Zhang, T.-K. Lau, T. Li, K. Liu, Q. Ling, C. Wang, X. Lu, W. You, X. Zhan, *J. Am. Chem. Soc.* 139 (2017) 1336.
- [15] S. Li, L. Ye, W. Zhao, S. Zhang, S. Mukherjee, H. Ade, J. Hou, *Adv. Mater* 28 (2016) 9423.
- [16] D. Liu, B. Yang, B. Jang, B. Xu, S. Zhang, C. He, H.Y. Woo, J. Hou, *Energy Environ. Sci.* 10 (2017) 546.
- [17] H. Yao, Y. Chen, Y. Qin, R. Yu, Y. Cui, B. Yang, S. Li, K. Zhang, J. Hou, *Adv. Mater* 28 (2016) 8283.
- [18] W. Zhao, S. Zhang, J. Hou, *Sci. China Chem.* 59 (2016) 1574.
- [19] Q. Wu, D. Zhao, A.M. Schneider, W. Chen, L. Yu, *J. Am. Chem. Soc.* 138 (2016) 7248.
- [20] Y. Zhong, M.T. Trinh, R. Chen, G.E. Purdum, P.P. Khlyabich, M. Sezen, S. Oh, H. Zhu, B. Fowler, B. Zhang, W. Wang, C.-Y. Nam, M.Y. Sfeir, C.T. Black, M.L. Steigerwald, Y.-L. Loo, F. Ng, X.Y. Zhu, C. Nuckolls, *Nat. Commun.* 6 (2015).
- [21] S.M. McAfee, J.M. Topple, I.G. Hill, G.C. Welch, *J. Mater. Chem. A* 3 (2015) 16393.
- [22] D. Meng, D. Sun, C. Zhong, T. Liu, B. Fan, L. Huo, Y. Li, W. Jiang, H. Choi, T. Kim, J.Y. Kim, Y. Sun, Z. Wang, A.J. Heeger, *J. Am. Chem. Soc.* 138 (2016) 375.
- [23] Y. Duan, X. Xu, H. Yan, W. Wu, Z. Li, Q. Peng, *Adv. Mater* 29 (2017) 1605115.
- [24] A. Zhang, C. Li, F. Yang, J. Zhang, Z. Wang, Z. Wei, W. Li, *Angew. Chem. Int. Ed.* 56 (2017) 2694.
- [25] F. Fernandez-Lazaro, N. Zink-Lorre, A. Sastre-Santos, *J. Mater. Chem. A* 4 (2016) 9336.
- [26] C. Li, H. Wonneberger, *Adv. Mater* 24 (2012) 613.
- [27] J. Zhao, Y. Li, H. Lin, Y. Liu, K. Jiang, C. Mu, T. Ma, J.Y. Lin Lai, H. Hu, D. Yu, H. Yan, *Energy Environ. Sci.* 8 (2015) 520.
- [28] X. Zhang, Z. Lu, L. Ye, C. Zhan, J. Hou, S. Zhang, B. Jiang, Y. Zhao, J. Huang, S. Zhang, Y. Liu, Q. Shi, Y. Liu, J. Yao, *Adv. Mater* 25 (2013) 5791.
- [29] S. Rajaram, R. Shivanna, S.K. Kandappa, K.S. Narayan, *J. Phys. Chem. Lett.* 3 (2012) 2405.
- [30] Y. Liu, J.Y.L. Lai, S. Chen, Y. Li, K. Jiang, J. Zhao, Z. Li, H. Hu, T. Ma, H. Lin, J. Liu, J. Zhang, F. Huang, D. Yu, H. Yan, *J. Mater. Chem. A* 3 (2015) 13632.
- [31] J. Lee, R. Singh, D.H. Sin, H.G. Kim, K.C. Song, K. Cho, *Adv. Mater* 28 (2016) 69.
- [32] W. Chen, X. Yang, G. Long, X. Wan, Y. Chen, Q. Zhang, *J. Mater. Chem. C* 3 (2015) 4698.
- [33] S.Y. Liu, C.H. Wu, C.Z. Li, S.Q. Liu, K.H. Wei, H.Z. Chen, A.K.Y. Jen, *Adv. Sci.* 2 (2015).
- [34] Y. Lin, Y. Wang, J. Wang, J. Hou, Y. Li, D. Zhu, X. Zhan, *Adv. Mater* 26 (2014) 5137.
- [35] Y. Liu, C. Mu, K. Jiang, J. Zhao, Y. Li, L. Zhang, Z. Li, J.Y.L. Lai, H. Hu, T. Ma, *Adv. Mater* 27 (2015) 1015.
- [36] F. Alghunaimi, B. Ghanem, N. Alaslai, R. Swaidan, E. Litwiller, I. Pinnau, *J. Membr. Sci.* 490 (2015) 321.
- [37] B.S. Ghanem, M. Pişkin, M. Durmuş, M.E. El-Khouly, S.Y. Al-Raqa, *Polyhedron* 90 (2015) 85.
- [38] Y. Han, Y. Jiang, C.-F. Chen, *Chin. Chem. Lett.* 24 (2013) 475.
- [39] E.H. Menke, V. Lami, Y. Vaynzof, M. Mastalerz, *Chem. Commun.* 52 (2016) 1048–1051.
- [40] P.B. Dzhevakov, M.A. Topchiy, D.A. Zharkova, O.S. Morozov, A.F. Asachenko, M.S. Nechaev, *Adv. Synth. Cata* 358 (2016) 977.
- [41] P.-O. Schwartz, L. Biniek, E. Zaborova, B. Heinrich, M. Brinkmann, N. Leclerc, S. Méry, *J. Am. Chem. Soc.* 136 (2014) 5981.
- [42] C. Zhang, C.-F. Chen, *J. Organ. Chem.* 71 (2006) 6626.
- [43] H. Zhao, Y.Y. Zhang, H. Xu, E.F. He, Z.L. Zhang, Q.M. Peng, R.J. Zhang, H.Q. Zhang, *Mater. Lett.* 161 (2015) 208.
- [44] M.J. Ahrens, L.E. Sinks, B. Rytchinski, W. Liu, B.A. Jones, J.M. Giaimo, A.V. Gusev, A.J. Goshe, D.M. Tiede, M.R. Wasielewski, *J. Am. Chem. Soc.* 126 (2004) 8284.
- [45] G.E. Park, H.J. Kim, S. Choi, D.H. Lee, M.A. Uddin, H.Y. Woo, M.J. Cho, D.H. Choi, *Chem. Commun.* 52 (2016) 8873.